

A Unified Framework to Super-Resolve Face Images of Varied Low Resolutions

Qiuyu Peng, Zifei Jiang, Yan Huang and Jingliang Peng

Abstract—The existing face image super-resolution (FSR) algorithms usually train a specific model for a specific low input resolution for optimal results. By contrast, we explore in this work a unified framework that is trained once and then used to super-resolve input face images of varied low resolutions. For that purpose, we propose a novel neural network architecture that is composed of three anchor auto-encoders, one feature weight regressor and a final image decoder. The three anchor auto-encoders are meant for optimal FSR for three pre-defined low input resolutions, or named anchor resolutions, respectively. An input face image of an arbitrary low resolution is firstly up-scaled to the target resolution by bi-cubic interpolation and then fed to the three auto-encoders in parallel. The three encoded anchor features are then fused with weights determined by the feature weight regressor. At last, the fused feature is sent to the final image decoder to derive the super-resolution result. As shown by experiments, the proposed algorithm achieves robust and state-of-the-art performance over a wide range of low input resolutions by a single framework. Code and models will be made available after the publication of this work.

I. INTRODUCTION

While face images are the core type of data underlying many applications, *e.g.*, video surveillance, face recognition, face alignment and face manipulation, the raw images were often acquired at low resolutions due to the limited picturing conditions. Therefore, it is often desired to raise the resolution of a raw face image to facilitate more successful applications. Correspondingly, the field of face image super-resolution (FSR), or sometimes by the name of face hallucination, has been intensively researched in recent years.

In general, it is a great challenge to faithfully restore the high resolution of a face image, particularly so as human eyes (and even computers) are sensitive to even minute distortions or artifacts in a reconstructed face image. In order to tackle this challenge, many algorithms have been proposed since the early 2000s. Initially, algorithms based on traditional machine learning techniques were proposed for the FSR task. Since 2015 or so, deep-learning-based FSR algorithms have become the main-stream, leading to great successes for typical up-scaling factors (*e.g.*, $\times 8$ and $\times 4$).

However, one issue with the existing FSR algorithms is that they usually optimize a model separately for each specific up-scaling factor. For deep-learning-based methods, this means that a separate neural network (NN) model should be trained and maintained for each specific up-scaling factor. This brings high computing and memory costs for training and maintaining different models for different up-scaling factors. In real application scenarios, this problem is exacerbated as face images may be captured at arbitrarily low resolutions, making it impractical to train and maintain a model for every possible low resolution.

In order to solve this issue, we explore super-resolving face images of arbitrary low resolutions in a unified way with a single model. Specifically, we propose in this work a novel neural network framework that is trained once and used to super-resolve input face images of varied low resolutions. The proposed method anchors the input image of an arbitrary resolution by auto-encoders to three features roughly corresponding to three pre-defined anchor resolutions, which are then fused and sent to an image decoder to derive the final result. Major contributions of this work reside in the following aspects.

- **Identification of the issue with rigid model-resolution binding.** To the best of our knowledge, for the problem of FSR, we explicitly point out the issue with rigid binding of optimal model and input image resolution and explore solutions for the first time.
- **Unified FSR framework for varied input resolutions.** We propose an original algorithm with a unified neural network framework that is trained for once and applied to super-resolve face images of varied resolutions.
- **Robust and state-of-the-art (SOTA) FSR performance.** As shown by experiments, the proposed algorithm achieves robust and state-of-the-art performance over a wide range of low input resolutions by a single generic model.

II. RELATED WORK

A. Face Image Super-Resolution

In early years, FSR algorithms [1], [42], [53], [64], [12], [56], [80], [21] are mostly based on traditional machine learning technology. In recent years, deep-learning-based approaches to FSR have achieved great successes. Zhou *et al.* [77] employ deep Bi-channel CNN for FSR. Yu and Porikli [67] use discriminative generative networks to generate realistic super-resolution (SR) images. Huang and Liu [20] develop a deep CNN for FSR with iterative back projection

Q. Peng, Z. Jiang and Y. Huang are all with School of Software, Shandong University, Jinan, Shandong, 250101, P. R. China. J. Peng is with Shandong Provincial Key Laboratory of Network Based Intelligent Computing & School of Information Science and Engineering, University of Jinan, Jinan, Shandong, 250022, P. R. China. Y. Huang and J. Peng are the corresponding authors.
E-mails: pengqiuyu@mail.sdu.edu.cn, jiangzifei@mail.sdu.edu.cn, yan.h@sdu.edu.cn, ise_pengjl@ujn.edu.cn.

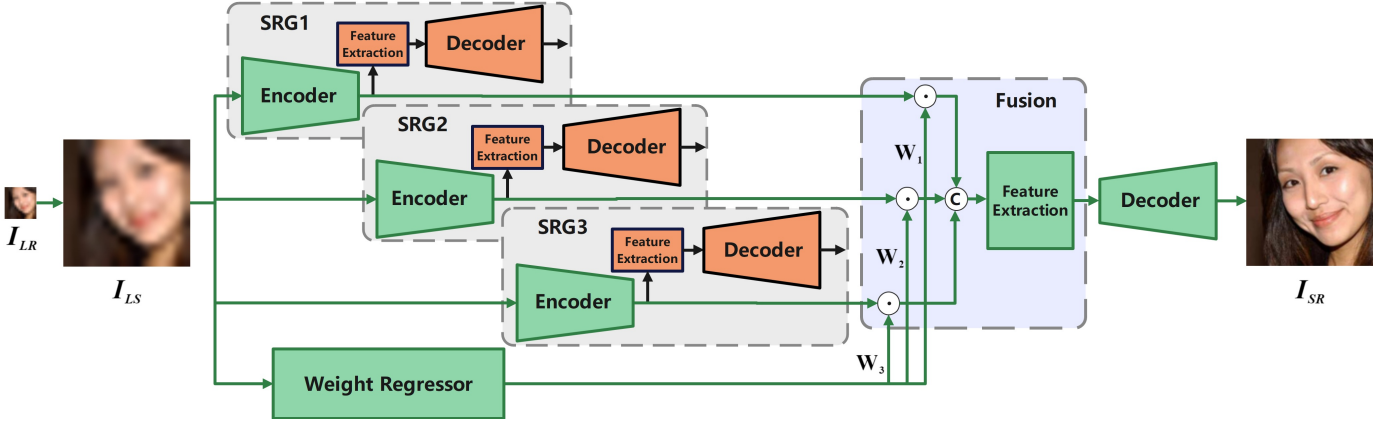


Fig. 1. Complete architecture of the proposed UFVNet, including modules and data flows for both training and testing. It is composed of three image encoder-decoders (or named anchor SR generators, SRGs), a weight regressor, a fusion module and a final decoder module. All the blocks and arrows (indicating data flows) are used in the training, while only the green blocks and arrows are kept for the testing.

introduced for extra post-processing. Huang *et al.* [22] propose a CNN to predict wavelet coefficients which are then used to reconstruct the high-resolution (HR) image. Jiang *et al.* [26] use multiple models to generate candidate SR results which are fused for the final result. Hu *et al.* [17] propose to predict a basic face and a compensation face and fuse them to derive the SR image. Lu *et al.* [48] propose a global-local fused network for FSR, paying special attention to high-frequency information. Chen *et al.* [5] construct an FSR network with face attention units that extend residual blocks with spatial attention branches. Jiang *et al.* [25] propose an FSR network to capture and fuse both global facial shape and local facial components for the result. Dastmalchi *et al.* [9] propose to extract the wavelet coefficients and use them with the feature map in different scales to derive the result.

As a specific type of objects, faces have a well-defined structure. As such, face prior knowledge has been exploited by many FSR algorithms to guide the image generation. Song *et al.* [58] and Jiang *et al.* [24] both propose to crop a face into components by the estimated landmarks and predict high-frequency details for the components. Chen *et al.* [7] propose an NN that estimates both image features and landmark heatmaps/parsing maps and uses them to generate the final result. Li *et al.* [35] propose a five-branch NN with each branch super-resolving one facial part. Yin *et al.* [66] propose an NN that jointly conducts facial landmark detection and tiny face super-resolution. Ma *et al.* [50] propose an NN that conducts the FSR by iterative collaboration between facial image recovery and facial component estimation. Zhang *et al.* [74] make a multi-stage NN that exploits enhanced facial boundaries for the FSR. Kalarot *et al.* [28] propose a multi-stage NN that makes facial component segmentation and patch cropping for the FSR. Li *et al.* [37] propose a two-stage framework and introduce face attributes and face boundaries information to promote the FSR. Kim *et al.* [31] propose an NN that conducts FSR based on face edge information and identity loss function. Zhuang *et al.* [79] propose an NN where an SR branch and a facial component estimation branch collaborate iteratively to generate the final result. Wang

et al. [60] propose to first learn face prior knowledge by a teacher FSR network and distill this knowledge to a student FSR network.

Note that the FSR algorithms reviewed above train an optimal model for a specific image up-scaling factor. Though some works (*e.g.* [48], [37], [5]) report results for multiple up-scaling factors, they train a separate model for each.

B. Scale-Arbitrary Image Super-Resolution

For generic images, research has been started on scale-arbitrary super-resolution (SASR) in the recent few years. Hu *et al.* [19] propose a meta-learning approach that dynamically predicts appropriate up-sampling filters for arbitrary magnification factors. Wang *et al.* [61] design a plug-in module for existing SR networks which consists of multiple scale-aware filters and a scale-aware up-sampling layer. Chen *et al.* [6] propose Local Implicit Image Function (LIIF) to predict the RGB value at any given image coordinate with the 2D deep features around the coordinate. Son *et al.* [57] propose an SRWarp model that can transform the LR image to match any shape of the HR image at the feature level.

Note that the SASR algorithms reviewed above are proposed for generic images but not optimized specifically for face images. In the field of FSR, we have found no similar algorithms published.

III. APPROACH

We propose a novel deep-learning-based unified framework that is trained for once and then used to super-resolve images of varied low resolutions. We name it UFVNet in a short form. The input image of an arbitrary resolution, $I_{LR} \in \mathbb{R}^{h \times w}$, is firstly scaled by bi-cubic interpolation to $I_{LS} \in \mathbb{R}^{H \times W}$ and then sent to the trained UFVNet to obtain the super-resolved image, $I_{SR} \in \mathbb{R}^{H \times W}$, where $h \times w$ and $H \times W$ are the sizes of the LR image and the SR image, respectively. The architecture of the complete UFVNet is shown in Fig. 1.

As shown in Fig. 1, the complete UFVNet is composed of three encoder-decoder branches, a weight regression branch, a feature fusion module and a final decoder module. Note that,

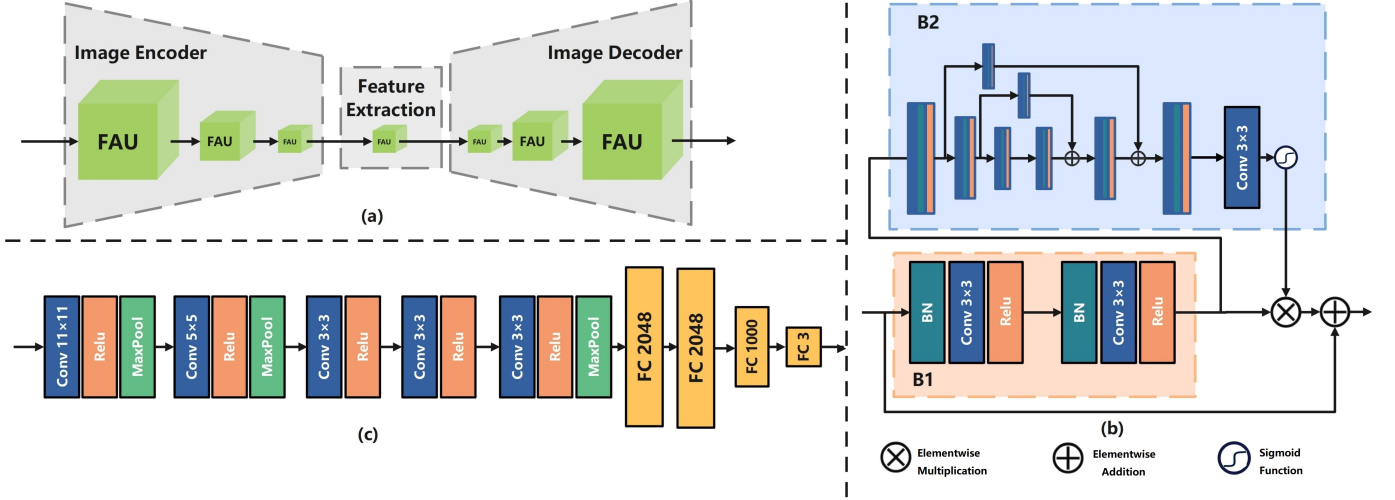


Fig. 2. Structural overview of (a) anchor SR generator, (b) FAU block and (c) weight regressor.

all the blocks in Fig. 1 are used for the training, while only the green blocks are kept for the testing. The encoder-decoder in each branch itself is a complete FSR network that means to work best by itself for a certain input image resolution called anchor resolution. As such, the whole branch is an anchor SR generator (SRG) and the encoder/decoder is called anchor encoder/decoder. We train the network such that the three encoder-decoder branches correspond to three different anchor resolutions, respectively, and the weight regressor automatically derives weights for the three encoded anchor features.

Detailed explanations of the structural components, the training process and the loss function are given in the following subsections.

A. Anchor SR Generator

Theoretically, any encoder-decoder based FSR model may be used as backbone for the three anchor SR generators in UFVNet. Among them, SPARNet [5] is of particular interest to us. Firstly, it is one of the state-of-the-art FSR models; secondly, it has a neatly defined encoder-decoder structure with no dependence on any face prior. Therefore, SPARNet fits our purpose of prototype neural network design very well.

In UFVNet, all the three anchor SR generators have the same network structure, as shown in Fig. 2(a). It is composed of an encoder with three face attention units (FAUs), a decoder also with three FAUs and one FAU in-between for further latent feature extraction. Note that we build the SR generator by adapting the original SPARNet [5]. The major adaptations include that we adopt a light version (*i.e.* SPARNet-Light-Attn3D [4]) released by the authors and that we use just one FAU for the latent feature extraction favoring a compact and efficient network. As for the FAU, we use the same structure as released [4], which is shown in Fig. 2(b). It is composed of a feature extraction block and a spatial attention block plus a residual connection for effective high-level and low-level feature extraction [5].

In essence, each anchor SR generator consists of seven FAUs in sequence. Denote the input and output of the t -th FAU as \mathbf{f}_{t-1} and \mathbf{f}_t , $1 \leq t \leq 7$, respectively, with $\mathbf{f}_0 = \mathbf{I}_{LS}$. The computing process of the t -th FAU is mathematically modeled as:

$$\mathbf{f}_t^{B_1} = B_1(\mathbf{f}_{t-1}), \quad (1)$$

$$\mathbf{f}_t^{B_2} = B_2(\mathbf{f}_t^{B_1}), \quad (2)$$

$$\mathbf{f}_t = \mathbf{f}_t^{B_1} \otimes \mathbf{f}_t^{B_2} \oplus \mathbf{f}_{t-1} \quad (3)$$

where $B_1(\cdot)$ and $B_2(\cdot)$ are the mapping functions of the feature block and the attention block, respectively, and \otimes and \oplus denote element-wise multiplication and element-wise addition, respectively.

B. Weight Regressor

Assume that we send the scaled input image \mathbf{I}_{LS} to each anchor SR generator separately, we would obtain three SR images. It is predictable that the best result would be mostly given by the anchor SR generator whose anchor resolution is the closest to the resolution of \mathbf{I}_{LR} . However, the resolution of \mathbf{I}_{LR} may not exactly match any one of the anchor resolutions. As such, we send \mathbf{I}_{LS} (scaled \mathbf{I}_{LR}) to all the three anchor encoders and make a weighted fusion of the encoded features to make a more robust and complete characterization of \mathbf{I}_{LS} . While a simple formula may be manually defined to map input resolution to anchor weights, we choose to design a neural network module for weight regression that can learn a more complex mapping adaptive to both resolution and content of \mathbf{I}_{LR} .

All the weights are non-negative and sum up to one. In general, we should assign a bigger weight to an anchor resolution closer to the input resolution. If we view the three anchor resolutions as cluster heads and weights as confidence values, weight computing turns out to be similar to soft classification of the input image by resolution. Therefore, we employ AlexNet, a concise image classifier, as the basis of our weight regressor. Upon the baseline, we modify the hyper-parameters of the first maxpooling layer to fit the size of \mathbf{I}_{LS} ,

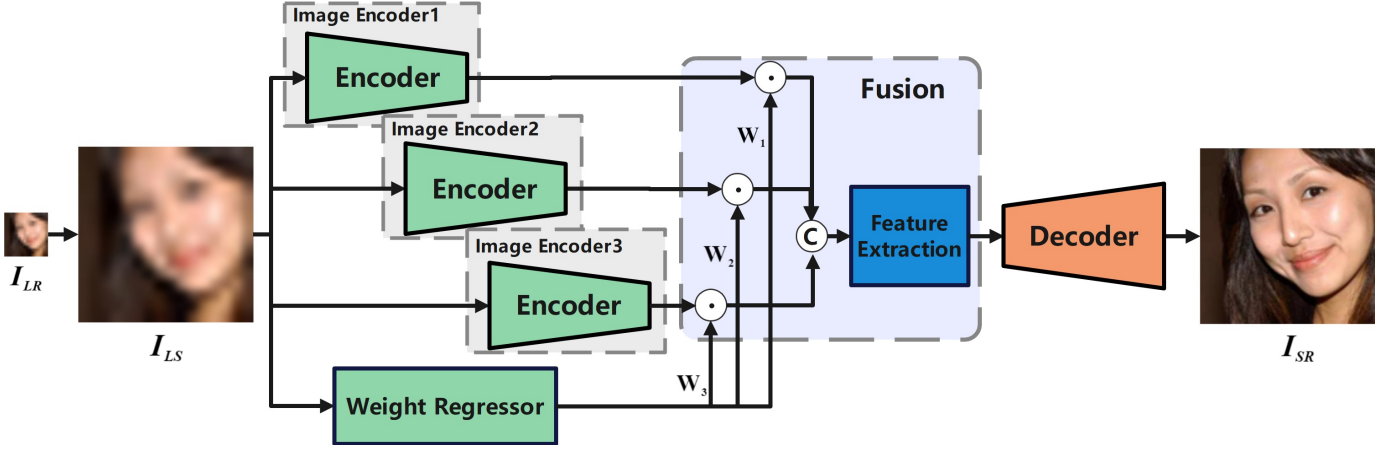


Fig. 3. The portion of the complete UFVNet that is used for the integrated training. When trained, it is also the model that is finally used in testing.

and add a fully-connected layer of three neurons at the end. The structure of the weight regressor is shown in Fig. 2(c).

C. Final Fusion and Decoding

At the end, the anchor features produced by the three anchor encoders are fused and decoded to generate the final SR image. As shown in Fig. 1, the fusion is accomplished by a weighted concatenation of the three encoded anchor features followed by another feature extraction block that is structurally the same as that in Fig. 2(a). Finally, the decoder at the end of the UFVNet also has the same structure as that in Fig. 2(a).

D. Training Process

All the blocks and data flows as shown in Fig. 1 participate in the training of UFVNet, and the training is conducted in two stages. Firstly, all the anchor SR generators and the weight regressor are separately trained; secondly, the modules pre-trained in the first stage are integrated and a portion of the UFVNet is trained further as a whole. For convenience, we also call the two stages separate training and integrated training, respectively.

We define the three anchor resolutions to be $\frac{1}{8}$, $\frac{1}{4}$ and $\frac{1}{2}$ the HR image size and train the anchor SR generators correspondingly. In order to generate the training LR images, we down-sample each HR image in the training set to $\frac{1}{8}$, $\frac{1}{4}$ and $\frac{1}{2}$ the original size via bi-cubic interpolation. For the three anchor SR generators, we use the $\frac{1}{8}$, $\frac{1}{4}$ and $\frac{1}{2}$ down-sampled LR images, respectively, and the corresponding HR images for the training. Each anchor SR generator is then trained as a stand-alone FSR model.

In order to train the weight regressor, we down-sample each HR image in the training set to eight low resolutions (i.e. $\frac{1}{16}$, $\frac{2}{16}$, $\frac{3}{16}$, $\frac{4}{16}$, $\frac{5}{16}$, $\frac{6}{16}$, $\frac{7}{16}$, $\frac{8}{16}$ the original HR image size) via bi-cubic interpolation. The weight regressor is then trained as a soft classifier. Denote the down-sampling rates of the three anchor resolutions as a_1 , a_2 and a_3 . Given an LR image with

down-sampling rate r , its class score $W = (w_1, w_2, w_3)$ is defined by

$$\begin{aligned} d_i &= |r - a_i|, 1 \leq i \leq 3, \\ w_i &= \frac{1}{2} \times \left(1 - \frac{d_i}{d_1 + d_2 + d_3}\right), 1 \leq i \leq 3. \end{aligned} \quad (4)$$

Finally, we integrate all the separately trained modules and further train a portion of the UFVNet as a whole. Note that, in this stage, the feature extraction and the decoder blocks of the anchor SR generators are discarded and the remaining portion of the UFVNet, as shown in Fig. 3, is trained by forward and backward propagations. After training, the neural network shown in Fig. 3 is then the final model used for testing.

In the following, we only formulate the forward propagation, from which the backward propagation may be derived. Denote the functions corresponding to the weight regressor, the three anchor encoders, the feature extraction block and the final decoder as F_{wt} , F_{enc1} , F_{enc2} , F_{enc3} , F_{FE} and F_{dec} , respectively. The whole mapping from the input \mathbf{I}_{LR} to the output \mathbf{I}_{SR} is formulated as

$$W = F_{wt}(U(\mathbf{I}_{LR})), \quad (5)$$

$$\mathbf{f}_{enc1} = F_{enc1}(U(\mathbf{I}_{LR})) \cdot W[1], \quad (6)$$

$$\mathbf{f}_{enc2} = F_{enc2}(U(\mathbf{I}_{LR})) \cdot W[2], \quad (7)$$

$$\mathbf{f}_{enc3} = F_{enc3}(U(\mathbf{I}_{LR})) \cdot W[3], \quad (8)$$

$$\mathbf{f}_{concat} = C(\mathbf{f}_{enc1}, \mathbf{f}_{enc2}, \mathbf{f}_{enc3}), \quad (9)$$

$$\mathbf{I}_{SR} = F_{dec}(F_{FE}(\mathbf{f}_{concat})) \quad (10)$$

where $W[i]$, $1 \leq i \leq 3$, denotes the i -th weight, $U(\cdot)$ denotes the up-scaling operation, and $C(\cdot)$ denotes the concatenation operation.

E. Loss Functions

In the separate training stage, L_1 loss is used for each SR generator and cross-entropy loss is used for the weight regressor. Denote the training LR-HR image pairs as $\{\mathbf{I}_{LR}^i, \mathbf{I}_{HR}^i\}_{i=1}^N$. For an SR generator (and the whole FSR neural network in Fig. 3), the loss is defined as

$$L^{SR} = \frac{1}{N} \sum_{i=0}^N |\mathbf{I}_{HR}^i - \mathbf{I}_{SR}^i|. \quad (11)$$

For the weight regressor, the loss is defined as

$$L^{wt} = \frac{1}{N} \sum_{i=0}^N L_{CE}(W_{GT}^i - W^i) \quad (12)$$

where W^i is the estimated weight vector and W_{GT}^i is the ground-truth weight vector (computed by Eq. 4) for \mathbf{I}_{LR}^i , and $L_{CE}(\cdot)$ denotes the cross-entropy loss function.

In the integrated training stage, the neural network shown in Fig. 3 is trained as a whole. The total loss is defined as

$$L^{total} = L^{SR} + \alpha L^{wt} \quad (13)$$

with L^{SR} and L^{wt} defined in Eq.s 11 and 12, respectively. We empirically set $\alpha = 0.1$ in the experiments.

IV. EXPERIMENTS

A. Implementation Details

Datasets and metrics: The datasets for training and testing in our experiments are variant from two prevalently used datasets: CelebA [47] and Helen [32]. We preprocess the images in the two datasets following the settings in Ma *et al.* [50]. Specifically, we crop the face images in the datasets with the files containing 68 key point position information of each face provided by [50], and resize the cropped images to 128×128 to obtain the HR images. We then scale the HR images to different low resolutions via bi-cubic interpolation and build up five multi-resolution data sets called CelebA-MR3, CelebA-MR7, CelebA-MR8, Helen-MR7 and Helen-MR8, respectively. There are three different low resolutions (*i.e.* $\frac{1}{8}$, $\frac{1}{4}$, $\frac{1}{2}$ of the original HR) in CelebA-MR3, seven (*i.e.* $\frac{2}{16}$, $\frac{3}{16}$, $\frac{4}{16}$, $\frac{5}{16}$, $\frac{6}{16}$, $\frac{7}{16}$, $\frac{8}{16}$ of the original HR) in CelebA-MR7 and Helen-MR7, and eight (*i.e.* $\frac{1}{16}$, $\frac{2}{16}$, $\frac{3}{16}$, $\frac{4}{16}$, $\frac{5}{16}$, $\frac{6}{16}$, $\frac{7}{16}$, $\frac{8}{16}$ of the original HR) in CelebA-MR8 and Helen-MR8. In each of these datasets, there is a balanced distribution of images among various resolutions. We also follow the same settings in [50], [78], [5] to divide the five variant datasets into training sets and testing sets. In all our experiments, we use the training set of CelebA-MR3, CelebA-MR7 or CelebA-MR8 for training and use the testing set of CelebA-MR7, CelebA-MR8, Helen-MR7 or Helen-MR8 for testing. We use PSNR and SSIM [63] to evaluate the quality of an SR image.

Training settings: For UFVNet, we set the batch size to 32, and fix the learning rate at 2×10^{-4} . We use Adam to optimize the model with $\beta_1 = 0.9$, $\beta_2 = 0.999$. Our models are implemented in PyTorch and run on NVIDIA RTX 2080Ti GPUs.

B. Comparison with the state-of-the-arts

The previously published FSR methods cannot natively support generating SR images from inputs of varied low resolutions with a single model. Some of the SOTA methods are designed for a fixed up-scaling factor and use face images at a fixed resolution as the input. The others scale an LR image of arbitrary size uniformly to the original resolution (of the HR image) before feeding it to the network and, as such, may theoretically super-resolve input images of various resolutions. But still, the authors usually train and test their models for

specific fixed input resolutions. For comprehensive evaluation, we conduct experiments to compare UFVNet with both FSR methods using fixed-resolution (FR) input and FSR methods using original-resolution (OR) input. Further, we compare UFVNet with SASR models that are originally proposed for generic images. For brevity, we refer to these benchmark methods as FR methods, OR methods and SASR methods, respectively.

Comparison with FR methods: The state-of-the-art FR methods we compare with include DIC [50], SISN [49], WIPA [9] and MLGDN [79]. They all achieve good performance with an $8\times$ up-scaling factor. Among these works, SISN [49] and WIPA [9] train separate models for more than one up-scaling factors and achieve better performance with a $4\times$ up-scaling factor. As such, we choose the $4\times$ models for SISN [49] and WIPA [9]. The DIC [50] model provided by the authors is trained on CelebA and we directly use it. The SISN [49], WIPA [9] and MLGDN [79] models provided by the authors are not trained on CelebA, and we train them on CelebA by ourselves. In this experiment, we test the benchmark FR models on both CelebA-MR8 and Helen-MR8. We resize each test image to the input resolution of each specific benchmark FR model using bicubic interpolation. For our proposed UFVNet, we train it on CelebA-MR8 and test it on both CelebA-MR8 and Helen-MR8 in this experiment. We resize each test image to the resolution of 128×128 before inputting it to UFVNet. In addition, we use bicubic interpolation as a baseline FSR approach for comparison.

The quantitative results on CelebA-MR8 and Helen-MR8 are listed in Tab. I. We clearly observe that UFVNet outperforms all the FR methods and the baseline Bicubic method significantly in both PSNR and SSIM. The results indicate that the FR methods may not super-resolve inputs of varied resolutions satisfactorily by a single model. We also notice that even the baseline Bicubic method surpasses all the FR methods. This again shows that the FR models are optimized for specific input resolutions but do not generalize well for super-resolving LR images of a large gamut of resolutions.

We visualize some SR image results produced by different methods in Fig 4. It clearly shows higher quality of SR images generated by UFVNet than by the others. Even at a very low input resolution of 8×8 , as shown in the first row, UFVNet still produces identifiable face images. We further show in Fig. 5 that the FR models (*e.g.* DIC, WIPA) generate better results when the input images have the resolutions for which

TABLE I
PSNR AND SSIM PERFORMANCE OF UFVNET AND THE BENCHMARK METHODS USING FIXED-RESOLUTION INPUT. IN EACH COLUMN, RESULT IN **BOLD** IS THE BEST.

Method	Dataset	Scale Factor	CelebA-MR8		Helen-MR8	
			PSNR \uparrow	SSIM \uparrow	PSNR \uparrow	SSIM \uparrow
Bicubic	-	-	27.71	0.7853	28.21	0.8238
DIC [50]	-	$8\times$	26.50	0.7604	25.99	0.7654
SISN [49]	-	$4\times$	27.45	0.7763	27.63	0.8067
WIPA [9]	-	$4\times$	26.75	0.7624	27.11	0.7994
MLGDN [79]	-	$8\times$	26.39	0.7569	25.76	0.7565
UFVNet(Ours)	-	-	29.46	0.8321	29.49	0.8446



Fig. 4. Visual results by UFVNet and the benchmark FR methods on example images from CelebA-MR8 and Helen-MR8.

TABLE II
PSNR AND SSIM PERFORMANCE OF UFVNET AND THE BENCHMARK METHODS USING ORIGINAL-RESOLUTION INPUT. IN EACH COLUMN, RESULT IN **BOLD** IS THE BEST.

Method \ Dataset	Trained on CelebA-MR8				Trained on CelebA-MR3			
	CelebA-MR8		Helen-MR8		CelebA-MR8		Helen-MR8	
	PSNR↑	SSIM↑	PSNR↑	SSIM↑	PSNR↑	SSIM↑	PSNR↑	SSIM↑
Bicubic	27.71	0.7853	28.21	0.8238	27.71	0.7853	28.21	0.8238
SPARNet [5]	29.20	0.8201	29.34	0.8406	28.73	0.8112	28.90	0.8325
EIPNet [31]	25.11	0.7152	24.84	0.7303	24.89	0.7073	24.59	0.7243
KDFSRNet [60]	26.49	0.7672	26.83	0.8041	26.49	0.7672	26.83	0.8041
UFVNet(Ours)	29.46	0.8321	29.49	0.8446	29.16	0.8241	29.46	0.8453

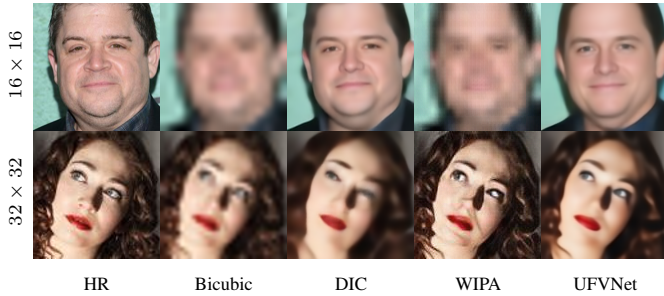


Fig. 5. More visual comparison for Bicubic, DIC, WIPA and UFVNet. DIC is originally trained for 16×16 input while WIPA for 32×32 input.

the models are originally trained. For other input resolutions, though, these models do not work optimally. But still, our UFVNet works robustly for the cases shown in Fig. 5.

Comparison with OR methods: The state-of-the-art OR methods we compare with include SPARNet [5], EIPNet [31] and KDFSRNet [60]. In this experiment, we make two settings for training and testing all the OR (except KDFSRNet) and UFVNet models: 1) training on CelebA-MR8 and testing on CelebA-MR8 and Helen-MR8, and 2) training on CelebA-MR3 and testing on CelebA-MR8 and Helen-MR8. It should be noted that KDFSRNet is published most recently with trained model but not training code released. Therefore, we use the trained model with a $4\times$ up-scaling factor for testing.

The quantitative results of this experiment are listed in Tab. II with results for the first settings on the left and the second settings on the right. We clearly observe that UFVNet achieves the best PSNR and SSIM performance among all the models in both settings. The performance gaps between all the OR and the Bicubic methods and UFVNet are

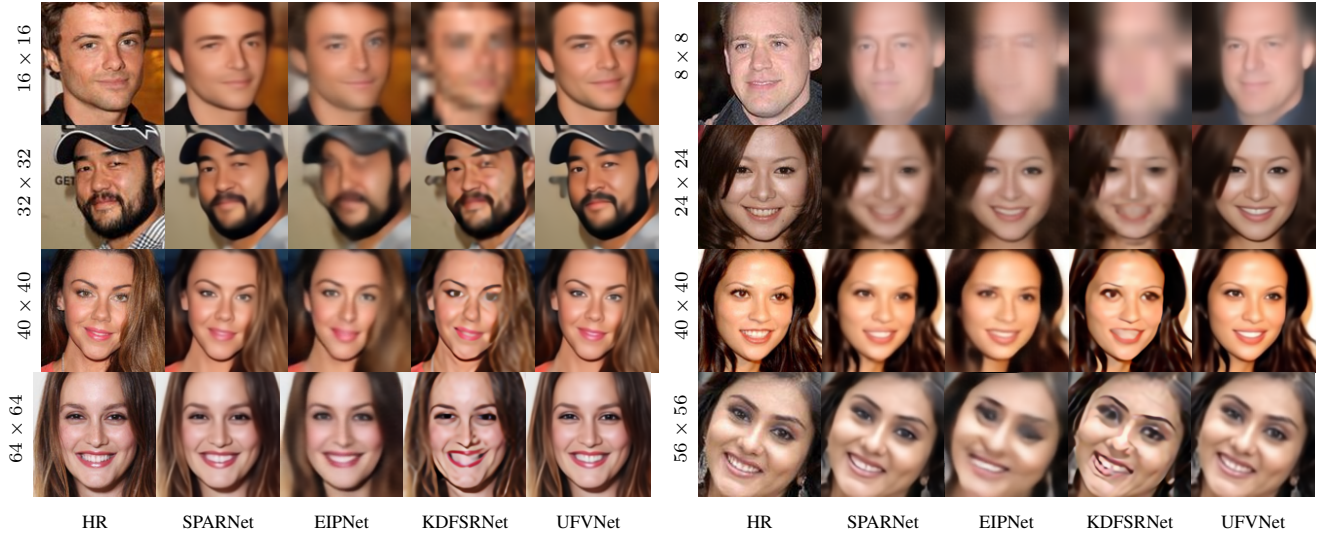


Fig. 6. Visual results by UFVNet and the benchmark OR methods on example images from CelebA-MR8 and Helen-MR8. Results on the left and the right halves are obtained by models trained on CelebA-MR8 and CelebA-MR3, respectively.

obvious. Among all the compared methods, SPARNet achieves performance closer to UFVNet, while EIPNet and KDFSRNet fall far behind. Referring to Tab. I, we find that EIPNet and KDFSRNet achieve metric values just close to those of the FR methods. This indicates that, without special design, these OR methods still cannot handle inputs of varied resolutions well. Further, we observe from Tab. II that, when the training dataset switches from CelebA-MR8 to CelebA-MR3, SPARNet and EIPNet suffer from larger performance drops than UFVNet. In other words, for input resolutions not seen in the training, UFVNet still performs comparably well while the other OR methods may perform obviously worse. This demonstrates the robustness and extensibility of UFVNet.

We visualize some SR image results produced by the OR methods and UFVNet in Fig. 6. It shows the superior performance of UFVNet in both experimental settings and across a wide range of input resolutions.

Comparison with SASR methods: We have found no FSR algorithm that processes inputs of varied resolutions with a single model. But still, we compare UFVNet with two representative SASR models, *i.e.* ArbSR [61] and LIIF [6], that were recently proposed for generic image super-resolution. For fairness of comparison, we train ArbSR, LIIF and UFVNet all on CelebA-MR7 and test them all on CelebA-MR7 and Helen-MR7. Note that we exclude the very low resolution, *i.e.* $\frac{1}{16}$ the original HR, from our training and testing datasets. This is to

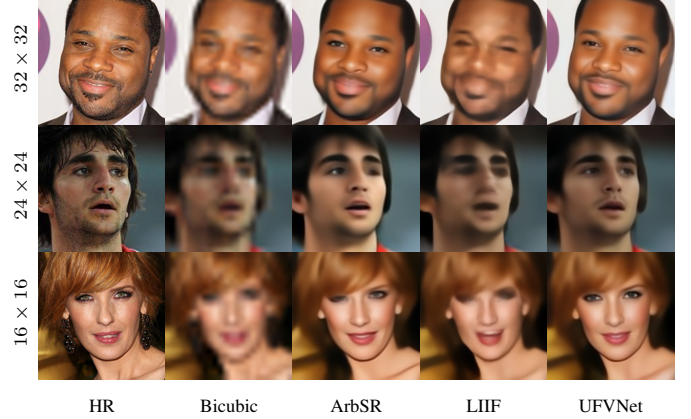


Fig. 7. Visual results by UFVNet and the benchmark SASR methods on example images from CelebA-MR7 and Helen-MR7.

avoid biased comparison as ArbSR and LIIF produce $16\times$ SR images of very poor quality on our datasets. For the training of ArbSR, LR images of various sizes are used as input and their corresponding 128×128 HR images are used as ground-truth. For the training of LIIF, ground-truth references are re-generated from training images by random scaling, which are down-sized to 16×16 images for input.

The quantitative results are listed in Tab. III. We clearly observe that UFVNet outperforms the SASR methods and the baseline Bicubic method significantly in both PSNR and SSIM. In addition, we visualize some SR image results of different methods in Fig. 7. From these examples, we observe that our proposed algorithm achieves clearly better quality of SR images than the others. This reflects the fact that the SASR methods are optimized for generic image SR but not so for specific FSR tasks.

TABLE III
PSNR AND SSIM PERFORMANCE OF THE BENCHMARK SASR METHODS AND UFVNET. IN EACH COLUMN, RESULT IN **BOLD** IS THE BEST.

Method \ Dataset	CelebA-MR7		Helen-MR7	
	PSNR \uparrow	SSIM \uparrow	PSNR \uparrow	SSIM \uparrow
Bicubic	28.75	0.8231	29.03	0.8464
ArbSR [61]	28.77	0.8540	28.82	0.8633
LIIF [6]	29.90	0.8449	30.13	0.8553
UFVNet(Ours)	30.43	0.8606	30.48	0.8663

TABLE IV

QUANTITATIVE COMPARISON OF THE SIX MODELS ON THE CELEBA AND THE HELEN DATASETS. IN EACH COLUMN, RESULT IN **BOLD** IS THE BEST.

Method \ Dataset	Trained on CelebA-MR8				Trained on CelebA-MR3			
	CelebA-MR8		Helen-MR8		CelebA-MR8		Helen-MR8	
	PSNR↑	SSIM↑	PSNR↑	SSIM↑	PSNR↑	SSIM↑	PSNR↑	SSIM↑
UFVNet-NW	29.25	0.8299	29.19	0.8410	28.89	0.8161	29.13	0.8378
UFVNet-FM	29.35	0.8310	29.45	0.8320	24.27	0.7612	24.21	0.7820
OneSRG	29.20	0.8201	29.34	0.8406	28.73	0.8112	28.90	0.8325
TwoSRG	29.40	0.8283	29.46	0.8430	28.80	0.8137	29.04	0.8342
FourSRG	29.48	0.8317	29.51	0.8436	28.64	0.8136	28.71	0.8346
UFVNet(Ours)	29.46	0.8321	29.49	0.8446	29.16	0.8241	29.46	0.8453

C. Ablation Study

The success of our unified framework in processing varied input face image resolutions is mainly due to two components of design, *i.e.* multiple anchor resolutions feature extraction and adaptive weight regression. In order to verify the effectiveness of these two key components, we conduct an ablation study in this subsection.

We make five additional models for the ablation study. UFVNet-NW is our network with the weight regression branch removed and the weights of the three encoder-decoder branches all fixed to 1. UFVNet-FM calculates the weights of the three encoder-decoder branches directly using the formulae in Eq.4. OneSRG, TwoSRG and FourSRG are the networks using one, two and four encoder-decoder branches, respectively. Besides, our proposed UFVNet, namely ThreeSRG, consists of three encoder-decoder branches.

We train all these models on the two training sets and test them on CelebA-MR8 and Helen-MR8. The results are shown in Tab. IV. We observe: 1) UFVNet significantly outperforms UFVNet-NW, UFVNet-FM and OneSRG, showing the effectiveness of both adaptive weight regression and multiple anchor resolutions feature extraction; 2) UFVNet (ThreeSRG) outperforms OneSRG, TwoSRG and FourSRG in overall performance, indicating that three encoder-decoder branches is the best choice.

V. CONCLUSION

In this work, we have proposed UFVNet, a unified framework to super-resolve face images of varied low resolutions. To the best of our knowledge, this is the first published framework of this type for the specific problem of FSR. The other existing FSR algorithms usually train a specific model for a specific low input resolution for optimal results but do not generalize well for super-resolving face images of varied resolutions.

The proposed UFVNet consists of three anchor branches each meant to work optimally for a pre-defined input resolution and a weight regression branch giving weights to combine the encoded features of the three anchor branches. Finally, the features are fused and fed to a final decoder to generate the final SR result. As experimentally demonstrated, the proposed FSR algorithm achieves superior performance over a large gamut of input resolutions by a single framework.

REFERENCES

- [1] Simon Baker and Takeo Kanade. Hallucinating faces. In *Proceedings Fourth IEEE international conference on automatic face and gesture recognition (Cat. No. PR00580)*, pages 83–88. IEEE, 2000.
- [2] Tadas Baltrusaitis, Amir Zadeh, Yao Chong Lim, and Louis-Philippe Morency. Openface 2.0: Facial behavior analysis toolkit. In *2018 13th IEEE international conference on automatic face & gesture recognition (FG 2018)*, pages 59–66. IEEE, 2018.
- [3] Nicolas Carion, Francisco Massa, Gabriel Synnaeve, Nicolas Usunier, Alexander Kirillov, and Sergey Zagoruyko. End-to-end object detection with transformers. In *European conference on computer vision*, pages 213–229. Springer, 2020.
- [4] Chaofeng Chen. Sparnet: Learning spatial attention for face super-resolution in pytorch. <https://github.com/chaofengc/Face-SPARNet>.
- [5] Chaofeng Chen, Dihong Gong, Hao Wang, Zhifeng Li, and Kwan-Yee K Wong. Learning spatial attention for face super-resolution. *IEEE Transactions on Image Processing*, 30:1219–1231, 2020.
- [6] Yinbo Chen, Sifei Liu, and Xiaolong Wang. Learning continuous image representation with local implicit image function. In *Proceedings of the IEEE/CVF conference on computer vision and pattern recognition*, pages 8628–8638, 2021.
- [7] Yu Chen, Ying Tai, Xiaoming Liu, Chunhua Shen, and Jian Yang. Fsrnet: End-to-end learning face super-resolution with facial priors. In *Proceedings of the IEEE Conference on Computer Vision and Pattern Recognition*, pages 2492–2501, 2018.
- [8] Kyunghyun Cho, Bart Van Merriënboer, Caglar Gulcehre, Dzmitry Bahdanau, Fethi Bougares, Holger Schwenk, and Yoshua Bengio. Learning phrase representations using rnn encoder-decoder for statistical machine translation. *arXiv preprint arXiv:1406.1078*, 2014.
- [9] Hamidreza Dastmalchi and Hassan Aghaeinia. Super-resolution of very low-resolution face images with a wavelet integrated, identity preserving, adversarial network. *Signal Processing: Image Communication*, page 116755, 2022.
- [10] Xuanyi Dong, Shou-I Yu, Xinshuo Weng, Shih-En Wei, Yi Yang, and Yaser Sheikh. Supervision-by-registration: An unsupervised approach to improve the precision of facial landmark detectors. In *Proceedings of the IEEE Conference on Computer Vision and Pattern Recognition*, pages 360–368, 2018.
- [11] Alexey Dosovitskiy, Lucas Beyer, Alexander Kolesnikov, Dirk Weissenborn, Xiaohua Zhai, Thomas Unterthiner, Mostafa Dehghani, Matthias Minderer, Georg Heigold, Sylvain Gelly, et al. An image is worth 16x16 words: Transformers for image recognition at scale. *arXiv preprint arXiv:2010.11929*, 2020.
- [12] Reuben A. Farrugia and Christine Guillemot. Face hallucination using linear models of coupled sparse support. *IEEE Transactions on Image Processing*, 26:4562–4577, 2017.
- [13] Ying Fu, Jian Chen, Tao Zhang, and Yonggang Lin. Residual scale attention network for arbitrary scale image super-resolution. *Neurocomputing*, 427:201–211, 2021.
- [14] Hang Zhao, Orazio Gallo, Iuri Frosio, Jan, and Kautz. Loss functions for image restoration with neural networks. *IEEE Transactions on Computational Imaging*, 2017.
- [15] Kaiming He, Xiangyu Zhang, Shaoqing Ren, and Jian Sun. Deep residual learning for image recognition. In *Proceedings of the IEEE conference on computer vision and pattern recognition*, pages 770–778, 2016.
- [16] Sepp Hochreiter and Jürgen Schmidhuber. Long short-term memory. *Neural computation*, 9(8):1735–1780, 1997.

- [17] Xiao Hu, Peirong Ma, Zhuohao Mai, Shaohu Peng, Zhao Yang, and Li Wang. Face hallucination from low quality images using definition-scalable inference. *Pattern Recognition*, 94:110–121, 2019.
- [18] Xiyuan Hu, Zhenfeng Fan, Xu Jia, Zhihui Li, Xuyun Zhang, Lianying Qi, and Zuxing Xuan. Towards effective learning for face super-resolution with shape and pose perturbations. *Knowledge-Based Systems*, 220:106938, 2021.
- [19] Xuecai Hu, Haoyuan Mu, Xiangyu Zhang, Zilei Wang, Tieniu Tan, and Jian Sun. Meta-sr: A magnification-arbitrary network for super-resolution. In *Proceedings of the IEEE/CVF conference on computer vision and pattern recognition*, pages 1575–1584, 2019.
- [20] Dongdong Huang and Heng Liu. Face hallucination using convolutional neural network with iterative back projection. In *Chinese Conference on Biometric Recognition*, pages 167–175. Springer, 2016.
- [21] Hua Huang, Hui He, Xin Fan, and Junping Zhang. Super-resolution of human face image using canonical correlation analysis. *Pattern Recognition*, 43:2532–2543, 2010.
- [22] Huaibo Huang, Ran He, Zhenan Sun, and Tieniu Tan. Wavelet-srnet: A wavelet-based cnn for multi-scale face super resolution. In *Proceedings of the IEEE International Conference on Computer Vision*, pages 1689–1697, 2017.
- [23] Junjun Jiang, Chenyang Wang, Xianming Liu, and Jiayi Ma. Deep learning-based face super-resolution: A survey. *ACM Computing Surveys*, 55(1), nov 2021.
- [24] Junjun Jiang, Yi Yu, Jinhui Hu, Suhua Tang, and Jiayi Ma. Deep cnn denoiser and multi-layer neighbor component embedding for face hallucination. *arXiv preprint arXiv:1806.10726*, 2018.
- [25] Kui Jiang, Zhongyuan Wang, Peng Yi, Tao Lu, Junjun Jiang, and Zixiang Xiong. Dual-path deep fusion network for face image hallucination. *IEEE Transactions on Neural Networks and Learning Systems*, 33:378–391, 2022.
- [26] Kui Jiang, Zhongyuan Wang, Peng Yi, Guangcheng Wang, Ke Gu, and Junjun Jiang. Atmfnet: Adaptive-threshold-based multi-model fusion network for compressed face hallucination. *IEEE Transactions on Multimedia*, 22(10):2734–2747, 2019.
- [27] Amin Jourabloo, Mao Ye, Xiaoming Liu, and Liu Ren. Pose-invariant face alignment with a single cnn. In *Proceedings of the IEEE International Conference on computer vision*, pages 3200–3209, 2017.
- [28] Ratheesh Kalarot, Tao Li, and Fatih Porikli. Component attention guided face super-resolution network: Cagface. In *Proceedings of the IEEE/CVF Winter Conference on Applications of Computer Vision*, pages 370–380, 2020.
- [29] Sithara Kanakaraj, V. K. Govindan, and Saidalavi Kalady. Face super resolution: A survey. *International Journal of Image, Graphics and Signal Processing*, 9:54–67, 2017.
- [30] Deokyun Kim, Minseon Kim, Gihyun Kwon, and Dae-Shik Kim. Progressive face super-resolution via attention to facial landmark. *arXiv preprint arXiv:1908.08239*, 2019.
- [31] Jonghyun Kim, Gen Li, Inyong Yun, Cheolkon Jung, and Joongkyu Kim. Edge and identity preserving network for face super-resolution. *Neurocomputing*, 446:11–22, 2021.
- [32] Vuong Le, Jonathan Brandt, Zhe Lin, Lubomir Bourdev, and Thomas S Huang. Interactive facial feature localization. In *European conference on computer vision*, pages 679–692. Springer, 2012.
- [33] Christian Ledig, Lucas Theis, Ferenc Huszár, Jose Caballero, Andrew Cunningham, Alejandro Acosta, Andrew Aitken, Alykhan Tejani, Johannes Totz, Zehan Wang, et al. Photo-realistic single image super-resolution using a generative adversarial network. In *Proceedings of the IEEE conference on computer vision and pattern recognition*, pages 4681–4690, 2017.
- [34] Jaewon Lee and Kyong Hwan Jin. Local texture estimator for implicit representation function. In *Proceedings of the IEEE/CVF Conference on Computer Vision and Pattern Recognition*, pages 1929–1938, 2022.
- [35] Ke Li, Bahetiyaer Bare, Bo Yan, Bailan Feng, and Chunfeng Yao. Face hallucination based on key parts enhancement. In *2018 IEEE International Conference on Acoustics, Speech and Signal Processing (ICASSP)*, pages 1378–1382. IEEE, 2018.
- [36] Mengyan Li, Yuechuan Sun, Zhaoyu Zhang, and Jun Yu. A coarse-to-fine face hallucination method by exploiting facial prior knowledge. In *2018 25th IEEE International Conference on Image Processing (ICIP)*, pages 61–65, 2018.
- [37] Mengyan Li, Zhaoyu Zhang, Jun Yu, and Chang Wen Chen. Learning face image super-resolution through facial semantic attribute transformation and self-attentive structure enhancement. *IEEE Transactions on Multimedia*, 23:468–483, 2020.
- [38] Yijun Li, Sifei Liu, Jimei Yang, and Ming-Hsuan Yang. Generative face completion. In *Proceedings of the IEEE conference on computer vision and pattern recognition*, pages 3911–3919, 2017.
- [39] Z. Li, Jinglei Yang, Zheng Liu, Xiaomin Yang, Gwanggil Jeon, and Wei Wu. Feedback network for image super-resolution. *2019 IEEE/CVF Conference on Computer Vision and Pattern Recognition (CVPR)*, pages 3862–3871, 2019.
- [40] Zhen Li, Jinglei Yang, Zheng Liu, Xiaomin Yang, Gwanggil Jeon, and Wei Wu. Feedback network for image super-resolution. In *Proceedings of the IEEE/CVF conference on computer vision and pattern recognition*, pages 3867–3876, 2019.
- [41] Bee Lim, Sanghyun Son, Heewon Kim, Seungjun Nah, and Kyoung Mu Lee. Enhanced deep residual networks for single image super-resolution. In *Proceedings of the IEEE conference on computer vision and pattern recognition workshops*, pages 136–144, 2017.
- [42] Ce Liu, Harry Shum, and Changshui Zhang. A two-step approach to hallucinating faces: global parametric model and local nonparametric model. *Proceedings of the 2001 IEEE Computer Society Conference on Computer Vision and Pattern Recognition. CVPR 2001*, 1:I–I, 2001.
- [43] Shuang Liu, Chengyi Xiong, Xiaodi Shi, and Zhirong Gao. Progressive face super-resolution with cascaded recurrent convolutional network. *Neurocomputing*, 449:357–367, 2021.
- [44] Sifei Liu, Jimei Yang, Chang Huang, and Ming-Hsuan Yang. Multi-objective convolutional learning for face labeling. In *Proceedings of the IEEE conference on computer vision and pattern recognition*, pages 3451–3459, 2015.
- [45] Ze Liu, Yutong Lin, Yue Cao, Han Hu, Yixuan Wei, Zheng Zhang, Stephen Lin, and Baining Guo. Swin transformer: Hierarchical vision transformer using shifted windows. In *Proceedings of the IEEE/CVF International Conference on Computer Vision*, pages 10012–10022, 2021.
- [46] Zhi-Song Liu, Wan-Chi Siu, and Yui-Lam Chan. Features guided face super-resolution via hybrid model of deep learning and random forests. *IEEE Transactions on Image Processing*, 30:4157–4170, 2021.
- [47] Ziwei Liu, Ping Luo, Xiaogang Wang, and Xiaoou Tang. Deep learning face attributes in the wild. In *Proceedings of the IEEE international conference on computer vision*, pages 3730–3738, 2015.
- [48] Tao Lu, Jiaming Wang, Junjun Jiang, and Yanduo Zhang. Global-local fusion network for face super-resolution. *Neurocomputing*, 387:309–320, 2020.
- [49] Tao Lu, Yuanzhi Wang, Yanduo Zhang, Yu Wang, Liu Wei, Zhongyuan Wang, and Junjun Jiang. Face hallucination via split-attention in split-attention network. In *Proceedings of the 29th ACM International Conference on Multimedia*, pages 5501–5509, 2021.
- [50] Cheng Ma, Zhenyu Jiang, Yongming Rao, Jiwen Lu, and Jie Zhou. Deep face super-resolution with iterative collaboration between attentive recovery and landmark estimation. In *Proceedings of the IEEE/CVF conference on computer vision and pattern recognition*, pages 5569–5578, 2020.
- [51] Huiyu Mo, Leibo Liu, Wenping Zhu, Shouyi Yin, and Shaojun Wei. Face alignment with expression-and pose-based adaptive initialization. *IEEE Transactions on Multimedia*, 21(4):943–956, 2018.
- [52] Alejandro Newell, Kaiyu Yang, and Jia Deng. Stacked hourglass networks for human pose estimation. In *European conference on computer vision*, pages 483–499. Springer, 2016.
- [53] Jeong-Seon Park and Seong-Wan Lee. An example-based face hallucination method for single-frame, low-resolution facial images. *IEEE Transactions on Image Processing*, 17:1806–1816, 2008.
- [54] Omkar M Parkhi, Andrea Vedaldi, and Andrew Zisserman. Deep face recognition. 2015.
- [55] Niki Parmar, Ashish Vaswani, Jakob Uszkoreit, Lukasz Kaiser, Noam Shazeer, Alexander Ku, and Dustin Tran. Image transformer. In *International conference on machine learning*, pages 4055–4064. PMLR, 2018.
- [56] Jingang Shi and Guoying Zhao. Face hallucination via coarse-to-fine recursive kernel regression structure. *IEEE Transactions on Multimedia*, 21:2223–2236, 2019.
- [57] Sanghyun Son and Kyoung Mu Lee. Srwarp: Generalized image super-resolution under arbitrary transformation. In *Proceedings of the IEEE/CVF conference on computer vision and pattern recognition*, pages 7782–7791, 2021.
- [58] Yibing Song, Jiawei Zhang, Shengfeng He, Linchao Bao, and Qingxiang Yang. Learning to hallucinate face images via component generation and enhancement. *arXiv preprint arXiv:1708.00223*, 2017.
- [59] Chenyang Wang, Junjun Jiang, and Xianming Liu. Heatmap-aware pyramid face hallucination. *2021 IEEE International Conference on Multimedia and Expo (ICME)*, pages 1–6, 2021.

- [60] Chenyang Wang, Junjun Jiang, Zhiwei Zhong, and Xianming Liu. Propagating facial prior knowledge for multi-task learning in face super-resolution. *IEEE Transactions on Circuits and Systems for Video Technology*, 2022.
- [61] Longguang Wang, Yingqian Wang, Zaiping Lin, Jungang Yang, Wei An, and Yulan Guo. Learning a single network for scale-arbitrary super-resolution. In *Proceedings of the IEEE/CVF international conference on computer vision*, pages 4801–4810, 2021.
- [62] Nannan Wang, Dacheng Tao, Xinbo Gao, Xuelong Li, and Jie Li. A comprehensive survey to face hallucination. *International Journal of Computer Vision*, 106:9–30, 2013.
- [63] Zhou Wang, Alan C Bovik, Hamid R Sheikh, and Eero P Simoncelli. Image quality assessment: from error visibility to structural similarity. *IEEE transactions on image processing*, 13(4):600–612, 2004.
- [64] Chih-Yuan Yang, Sifei Liu, and Ming-Hsuan Yang. Structured face hallucination. *2013 IEEE Conference on Computer Vision and Pattern Recognition*, pages 1099–1106, 2013.
- [65] Jian Yang, Lei Luo, Jianjun Qian, Ying Tai, Fanlong Zhang, and Yong Xu. Nuclear norm based matrix regression with applications to face recognition with occlusion and illumination changes. *IEEE transactions on pattern analysis and machine intelligence*, 39(1):156–171, 2016.
- [66] Yu Yin, Joseph Robinson, Yulun Zhang, and Yun Fu. Joint super-resolution and alignment of tiny faces. In *Proceedings of the AAAI Conference on Artificial Intelligence*, volume 34, pages 12693–12700, 2020.
- [67] Xin Yu and Fatih Porikli. Ultra-resolving face images by discriminative generative networks. In *European conference on computer vision*, pages 318–333. Springer, 2016.
- [68] Amir Zadeh, Yao Chong Lim, Tadas Baltrusaitis, and Louis-Philippe Morency. Convolutional experts constrained local model for 3d facial landmark detection. In *Proceedings of the IEEE International Conference on Computer Vision Workshops*, pages 2519–2528, 2017.
- [69] Xianfang Zeng, Jiangning Zhang, Liang Liu, Guangzhong Tian, and Yong Liu. Selfsr: Self-conditioned face super-resolution in the wild via flow field degradation network. *arXiv preprint arXiv:2112.10683*, 2021.
- [70] Han Zhang, Ian J. Goodfellow, Dimitris N. Metaxas, and Augustus Odena. Self-attention generative adversarial networks. *ArXiv*, abs/1805.08318, 2019.
- [71] Menglei Zhang and Qiang Ling. Supervised pixel-wise gan for face super-resolution. *IEEE Transactions on Multimedia*, 23:1938–1950, 2020.
- [72] Yang Zhang, Xin Yu, Xiaobo Lu, and Ping Liu. Pro-uigan: Progressive face hallucination from occluded thumbnails. *IEEE Transactions on Image Processing*, 31:3236–3250, 2022.
- [73] Yulun Zhang, Yapeng Tian, Yu Kong, Bineng Zhong, and Yun Fu. Residual dense network for image super-resolution. In *Proceedings of the IEEE conference on computer vision and pattern recognition*, pages 2472–2481, 2018.
- [74] Yunchen Zhang, Yi Wu, and Liang Chen. Msfsr: A multi-stage face super-resolution with accurate facial representation via enhanced facial boundaries. In *Proceedings of the IEEE/CVF Conference on Computer Vision and Pattern Recognition Workshops*, pages 504–505, 2020.
- [75] Tianyu Zhao and Changqing Zhang. Saan: Semantic attention adaptation network for face super-resolution. In *2020 IEEE International Conference on Multimedia and Expo (ICME)*, pages 1–6. IEEE, 2020.
- [76] Erjin Zhou, Haoqiang Fan, Zhimin Cao, Yuning Jiang, and Qi Yin. Extensive facial landmark localization with coarse-to-fine convolutional network cascade. In *Proceedings of the IEEE international conference on computer vision workshops*, pages 386–391, 2013.
- [77] Erjin Zhou, Haoqiang Fan, Zhimin Cao, Yuning Jiang, and Qi Yin. Learning face hallucination in the wild. In *Twenty-ninth AAAI conference on artificial intelligence*, 2015.
- [78] Shizhan Zhu, Sifei Liu, Chen Change Loy, and Xiaoou Tang. Deep cascaded bi-network for face hallucination. In *European conference on computer vision*, pages 614–630. Springer, 2016.
- [79] Cheng Zhuang, Minqi Li, Kaibing Zhang, Zheng Li, and Jian Lu. Multi-level landmark-guided deep network for face super-resolution. *Neural Networks*, 152:276–286, 2022.
- [80] Yueting Zhuang, Jian Zhang, and Fei Wu. Hallucinating faces: Lph super-resolution and neighbor reconstruction for residue compensation. *Pattern Recognition*, 40:3178–3194, 2007.